Design, Simulation, Experimental Testing and Analysis of a Small-Scale 3D-Printed Horizontal Axis Wind Turbine

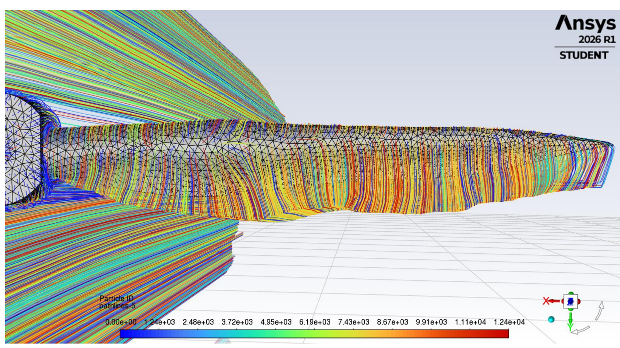

Mohammad Yaameen Zafar
yaameenzafar2507@gmail.com

Table of contents

Table of Figures

List of Abriviations

Abbreviation	Full Term
IRENA	International Renewable Energy Agency
CAD	Computer Aided Design
CFD	Computational Fluid Dynamics
Cm	Moment Coefficient
Cp	Power Coefficient
CSV	Comma-Separated Values
DC	Direct Current
FDM	Fused Deposition Modelling
HAWT	Horizontal Axis Wind Turbine
MPPT	Maximum Power Point Tracking
MRF	Multiple Reference Frame
PMSG	Permanent Magnet Synchronous Generator
SST	Shear Stress Transport
TSR	Tip Speed Ratio

Abstract

This report presents the design and analysis of a small-scale three-bladed horizontal axis wind turbine (HAWT). The turbine blades were designed in Autodesk Fusion 360 [4] with the NACA 4412 aerofoil profile [1] in mind, selected for its favourable lift-to-drag ratio at low Reynolds numbers, and manufactured via FDM 3D printing. Computational fluid dynamics (CFD) analysis was subsequently performed in ANSYS Fluent using a steady-state Multiple Reference Frame (MRF) approach with the k-omega SST turbulence model. An inlet wind velocity of 6.26 m/s was used, derived from the airflow specification of the Clarke CPF18B industrial fan [7] used during testing. CFD predicted an aerodynamic power output of 2,476 mW at the optimal operating speed of 370 rad/s (3,534 RPM), corresponding to a power coefficient of 0.514 — 86.8% of the theoretical Betz limit. A brushed DC motor was used as a generator, with electrical output measured using an INA219 current/voltage sensor [2] interfaced with an Arduino Uno R3, logging data at one-second intervals over a 200-second test period. The experimental apparatus produced a mean electrical power output of 58.73 mW. Primary losses were attributed to operating speed mismatch, generator inefficiency at low rotational speeds, and turbulent near-field fan airflow.

1 Introduction

Wind energy is one of the fastest-growing renewable energy sources globally, offering a clean alternative to fossil fuels across both utility scale and small distributed generation applications [3]. Small-scale horizontal axis wind turbines (HAWTs) provide an effective platform for studying the fundamental aerodynamic and electromechanical principles that govern energy conversion from wind to electricity, that can be operated at a large scale.

This project involved the end-to-end development of a miniature three-bladed HAWT. The blade geometry was first designed in Autodesk Fusion 360 following the NACA 4412 aerofoil profile, before CFD analysis was performed in ANSYS Fluent to predict aerodynamic performance. The turbine was then physically built and tested in airflow generated by a Clarke CPF18B industrial fan, with electrical output logged automatically via an Arduino Uno R3 and INA219 sensor. These results where then followed up in MATLAB where I was able to visualize the data, and obtain maximums and averages of the current, voltage and power generated in the turbine.

The objectives of this project were to: design aerodynamically informed turbine blades; simulate fluid behaviour using CFD; measure real electrical output using sensor hardware; and compare experimental results against theoretical predictions to evaluate system performance and identify key reasons for the losses observed between both the theoretical and optimal powers.

2 Theory

2.1 Aerodynamic Theory of Wind Turbine Blades

Wind approaches the turbine axially, parallel to the rotational axis, striking the front face of the rotor disc. The blades rotate in a plane perpendicular to this incoming flow. As a result, each blade section simultaneously experiences two velocity components: the free-stream wind velocity v acting axially, and the blade's own rotational velocity, ωr acting tangentially in the plane of rotation (opposing the direction of blade travel). The vector sum of these two components defines the relative wind velocity seen by that blade section, arriving at a flow angle φ to the plane of rotation [5]:

$$\varphi = arctan\left(\frac{v}{\omega r}\right)$$

The blade is twisted along its span so that the relative wind strikes the aerofoil at an appropriate angle of attack α at each section, this pitch and twist distribution is important to efficient operation across the full blade length.

Once the relative wind meets the aerofoil, aerodynamic lift and drag are generated. The cambered NACA 4412 profile accelerates airflow over the curved suction surface and decelerates it over the flatter pressure surface, producing a pressure differential by Bernoulli's principle [5]. This creates a lift force L perpendicular to the relative wind and a drag force D parallel to it:

$$L = C_L \times ½\rho {v_{rel}}^2 A$$
$$D = C_D \times ½\rho {v_{rel}}^2 A$$

Resolving these forces relative to the plane of rotation gives:

- Tangential force (drives torque): $F_T = L\, sin(\varphi) - D\, cos(\varphi)$
- Axial thrust (acts on tower structure): $F_A = L\, cos(\varphi) + D\, sin(\varphi)$

The torque driving the generator shaft is therefore $T = F_T \times r$, integrated across the blade span. Maximising F_T requires a high lift-to-drag ratio ($\frac{C_L}{C_D}$), a well-chosen angle of attack, and correct blade twist, all of which informed the NACA 4412 selection and blade geometry in this project.

2.2 Three Blade Orientation Justification

The number of blades on a HAWT directly affects aerodynamic efficiency, structural behaviour, and cost. While increasing the number of blades increases the solidity of the rotor (the fraction of the swept area covered by blades), the relationship between blade number and power coefficient Cp is non-linear [6].

A single blade reaches maximum Cp at very high TSR and suffers significant dynamic imbalance. Two blades are cheaper and lighter but produce asymmetric loading as they pass the tower, causing vibration and fatigue. Four or more blades approach their maximum Cp at much lower TSR, which suits slow-turning, high-torque applications such as water-pumping windmills, but is less efficient for electricity generation at typical wind speeds.

Three blades represent the engineering optimum for electricity-generating HAWTs for several reasons [6]:

- They achieve near-maximum Cp at the optimal TSR of approximately 6, without the diminishing returns of additional blades
- The symmetric three-point arrangement provides inherent rotational balance, minimising vibration and gyroscopic loading on the shaft and bearings
- An odd number of blades avoids structural resonance when a blade passes the tower, which occurs with two and four-blade designs
- Three blades are the established industry standard for commercial wind turbines globally, validating this choice for the present design

2.3 Tip Speed Ratio

The Tip Speed Ratio (λ) is the ratio of the blade tip speed to the free-stream wind velocity [7]:

$\lambda = \omega R / v$

For a three-bladed HAWT, the optimal TSR for maximum power extraction is approximately $\lambda = 6$. At this TSR and $v = 6.26$ m/s we only need the length of the designed blade to then complete the calculation, with a tip radius of 101mm, the value we obtain is 372 rad/s

2.4 NACA 4412 Aerofoil

The NACA 4412 aerofoil was used as the blade cross-section. The designation indicates 4% maximum camber at 40% chord, with 12% maximum thickness [1].]. The NACA 4412 aerofoil has well-documented lift and drag characteristics at low Reynolds numbers [1], making it a suitable choice for small-scale, low-speed turbine applications such as this.

2.5 Betz Limit and Wind Power

The total power available in a wind stream passing through a rotor swept area A at velocity v is given by the wind power equation [5]:

$$P_{wind} = ½\rho A v^3$$

where ρ is air density (1.225 kg/m³), A is the swept area (m²), and v is the free-stream wind velocity (m/s). The cubic relationship with velocity is significant — doubling wind speed produces eight times the available power. For this turbine (R = 101 mm, v = 6.26 m/s):

$$A = \pi R^2 = \pi \times 0.101^2 = 0.03205\, m^2$$

$$P_{wind} = 0.5 \times 1.225 \times 0.03205 \times 6.26^3 = 4{,}815\, mW$$

However, no turbine can extract all of this energy, the air must retain momentum to continue flowing through the rotor. Betz derived that the maximum fraction any turbine can extract is 59.3% [6], known as the Betz limit:

$$P_{Betz} = 0.593 \times 4{,}815 = 2{,}854\, mW$$

This sets the upper theoretical bound against which the CFD prediction and measured output are later compared.

3 Blade Design / Dimensions

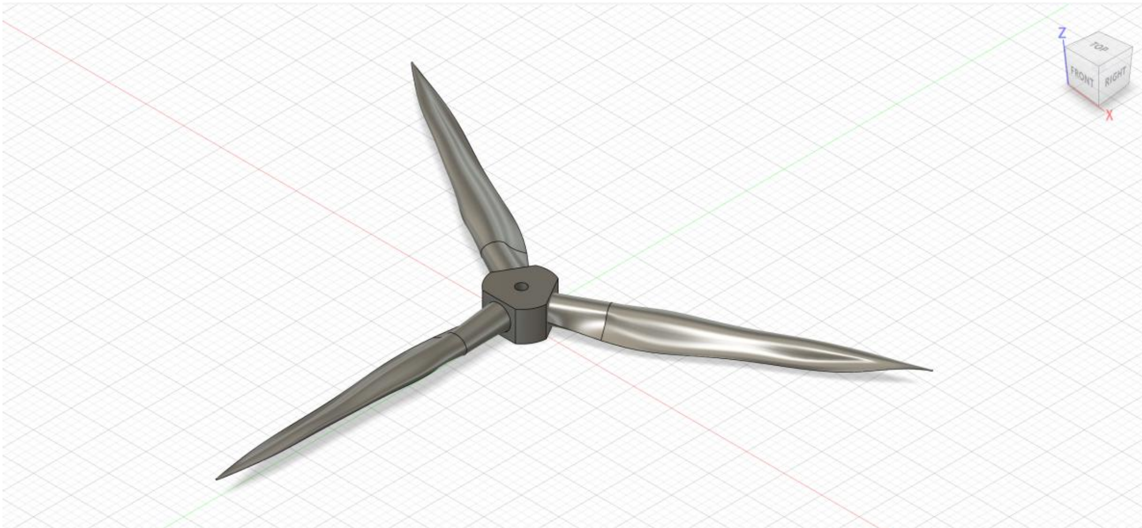

Figure 1: Orthographic View of Blade design

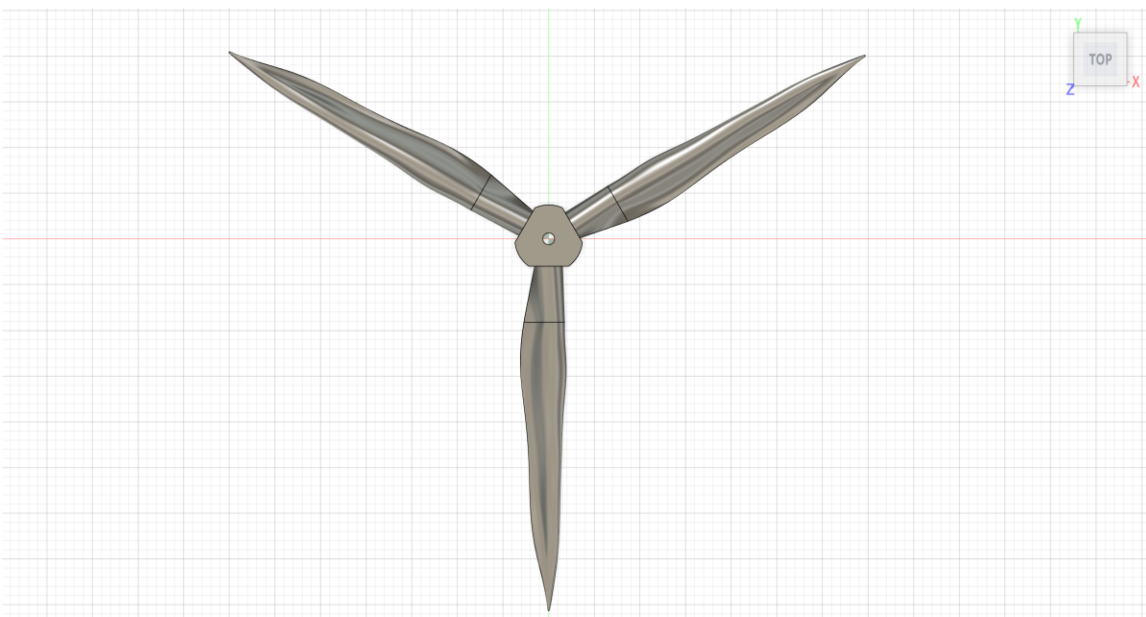

Figure 2: Plan View of Blades Design

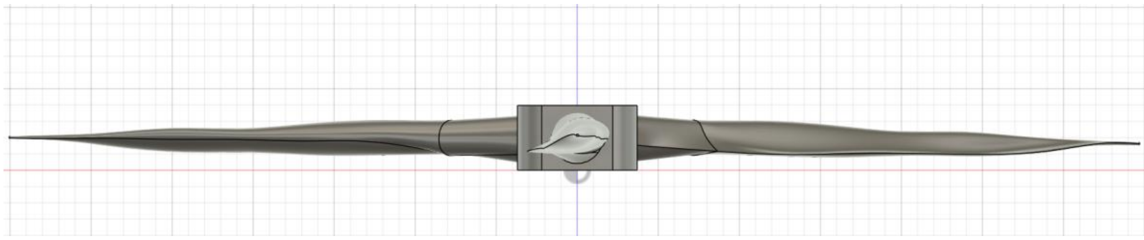

Figure 3: Side View of Blade Design

The final blade design has a span of 95 mm from root to tip. Combined with a hub radius of 5.97 mm, this gives a total tip radius of R = 101 mm. This span was the maximum achievable on the Bambu Lab A1 printer used for manufacture, with all components printed in PLA.

An earlier iteration of the blade was tested with a shorter span of 63 mm root to tip. This design was revised and extended to the 95 mm version to maximise the swept area and available wind power, while remaining within the printer's build volume constraints. A slight twist was applied along the blade span in Fusion 360. This accounts for the variation in relative wind angle between the root and tip, as discussed in Section 3.1.

4 CFD Simulation

4.1 Overview

Computational Fluid Dynamics analysis was performed in ANSYS Fluent 2026 to predict the torque of the turbine under realistic operating conditions. This result would then be used to calculate the estimated power output. The simulation used a Multiple Reference Frame (MRF) steady-state approach with the k-omega SST turbulence model and a Coupled pressure-velocity scheme, run over 200 iterations at 370 rad/s

4.2 Boundary Conditions

The inlet wind velocity was set to 6.26 m/s. The inlet wind velocity was determined from the Clarke CPF18B fan specifications. The fan has an outlet diameter of 18 inches (0.457 m) and a quoted volumetric flow rate of Q = 61.6 m^3/min. Converting to SI units and applying the continuity equation:

$$Q = 61.6 \div 60 = 1.027\, m^3/s$$

$$A_{fan} = \pi \times \left(\frac{0.457}{2}\right)^2 = 0.1641\, m^2$$

$$v = \frac{Q}{A} = \frac{1.027}{0.1641} = 6.26\, m/s$$

All other domain boundaries were set to pressure outlet conditions.

The rotational speed was set to 370 rad/s (3,534 RPM). This was derived from the optimal Tip Speed Ratio of $\lambda = 6$ for a three-bladed HAWT (Section 3.3), applied to the blade tip radius of R = 101 mm and inlet velocity of 6.26 m/s. Running the simulation at this speed ensures the CFD result represents peak theoretical performance, providing the strongest possible baseline for comparison.

4.3 Convergence

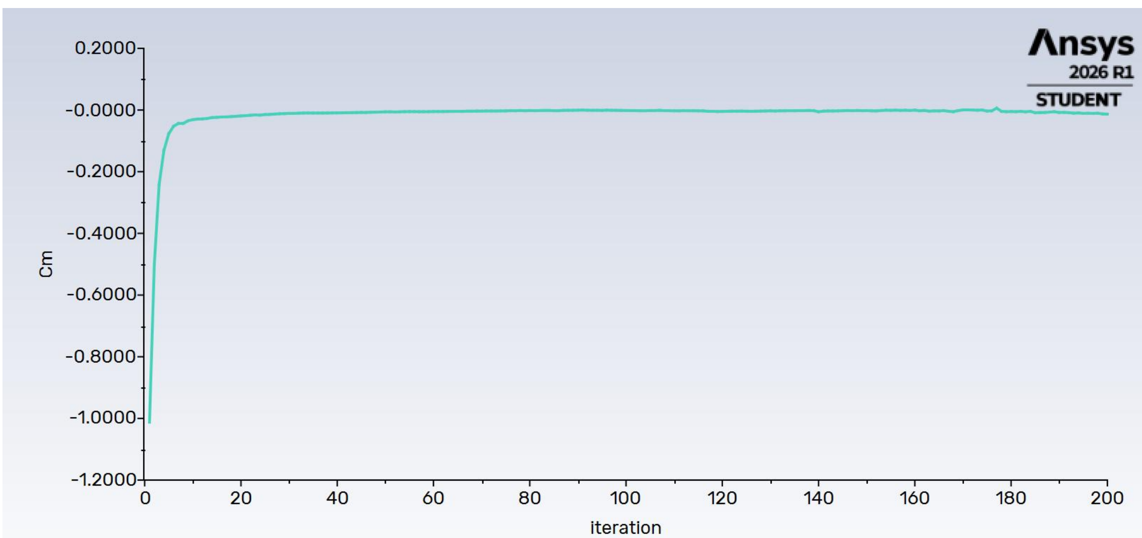

Figure 4: Cm monitor Plot

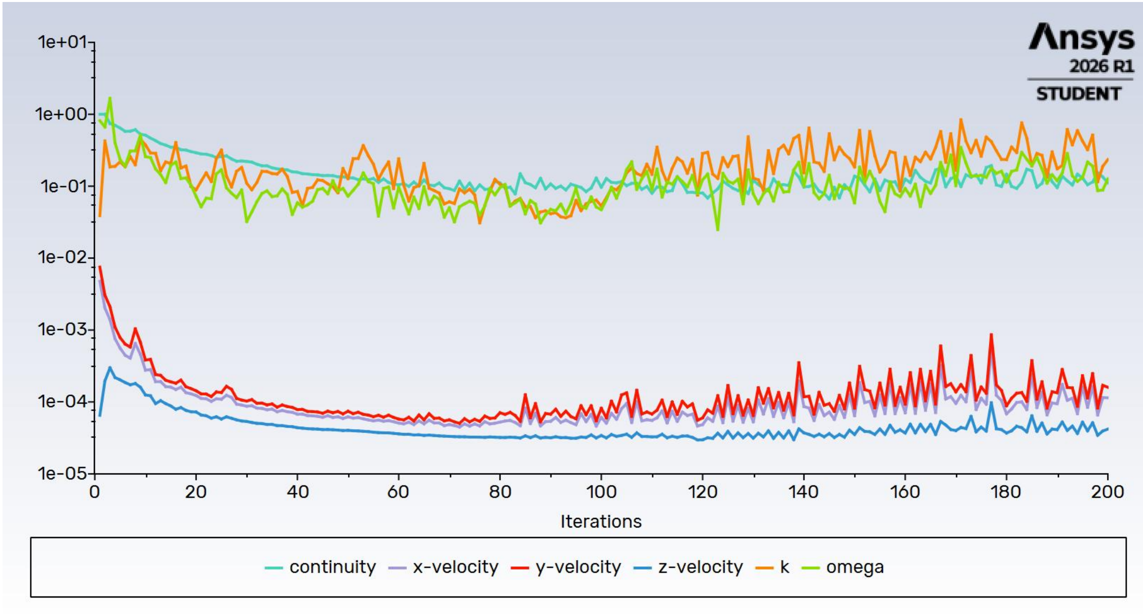

Figure 5: Residuals Plot

The moment coefficient (Cm) monitor converged to a flat, stable value from approximately iteration 20 and remained constant through to iteration 200. While the k and omega residuals show oscillation typical of rotating machinery simulations, the Cm convergence confirms the torque result is fully settled.

4.4 Flow Visualisation

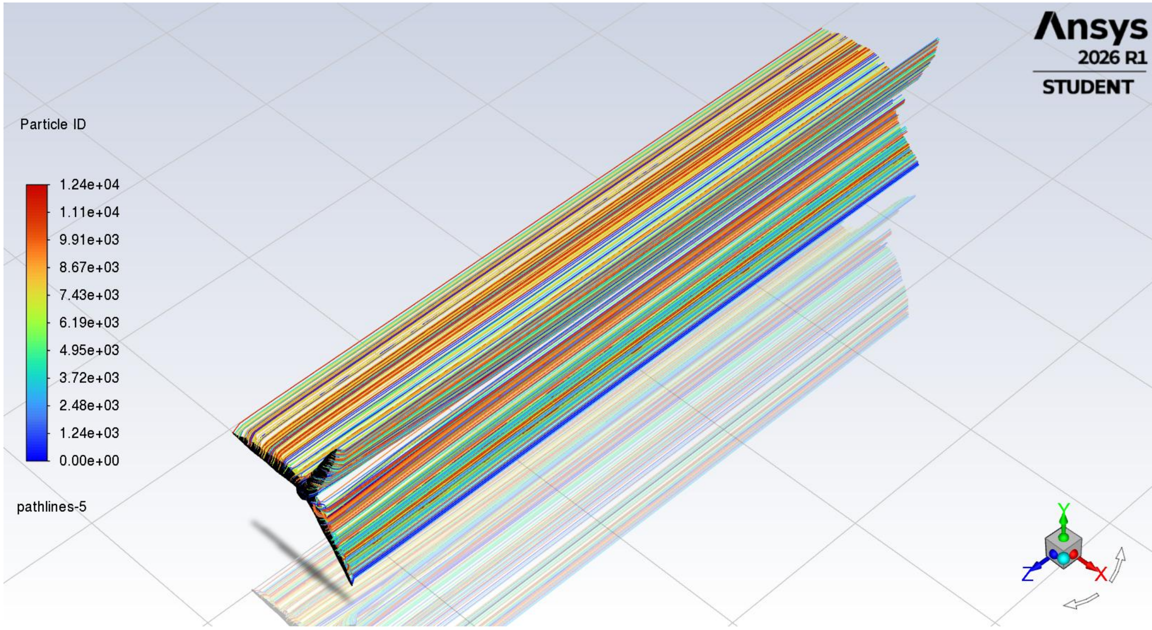

Figure 6: Isometric View of Pathlines

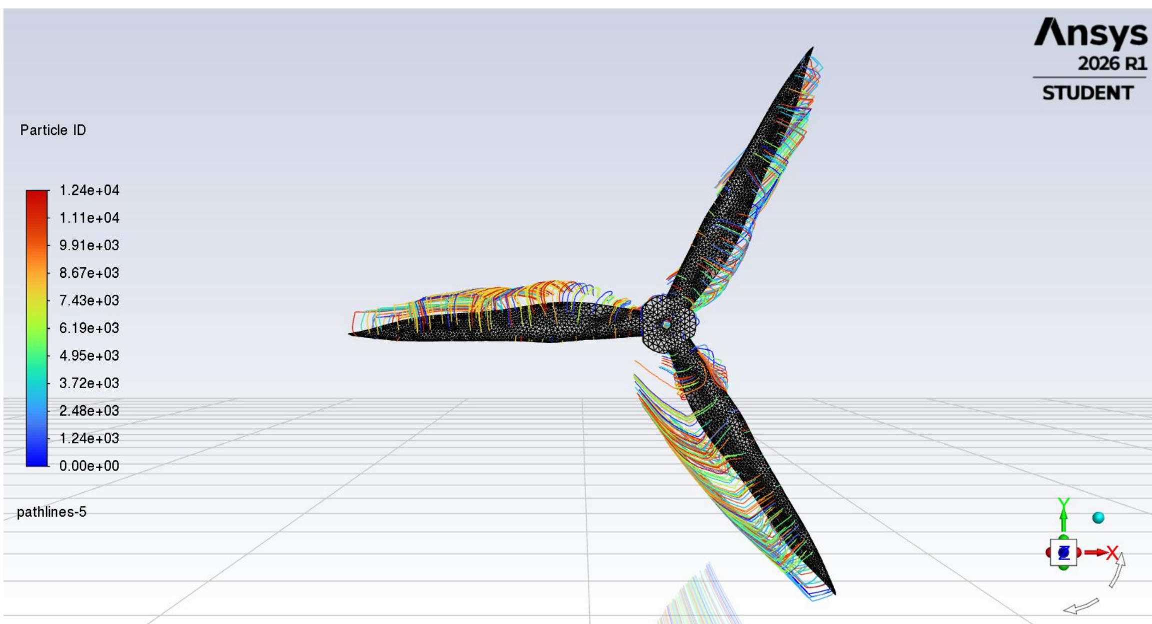

Figure 7: Front view of Pathlines

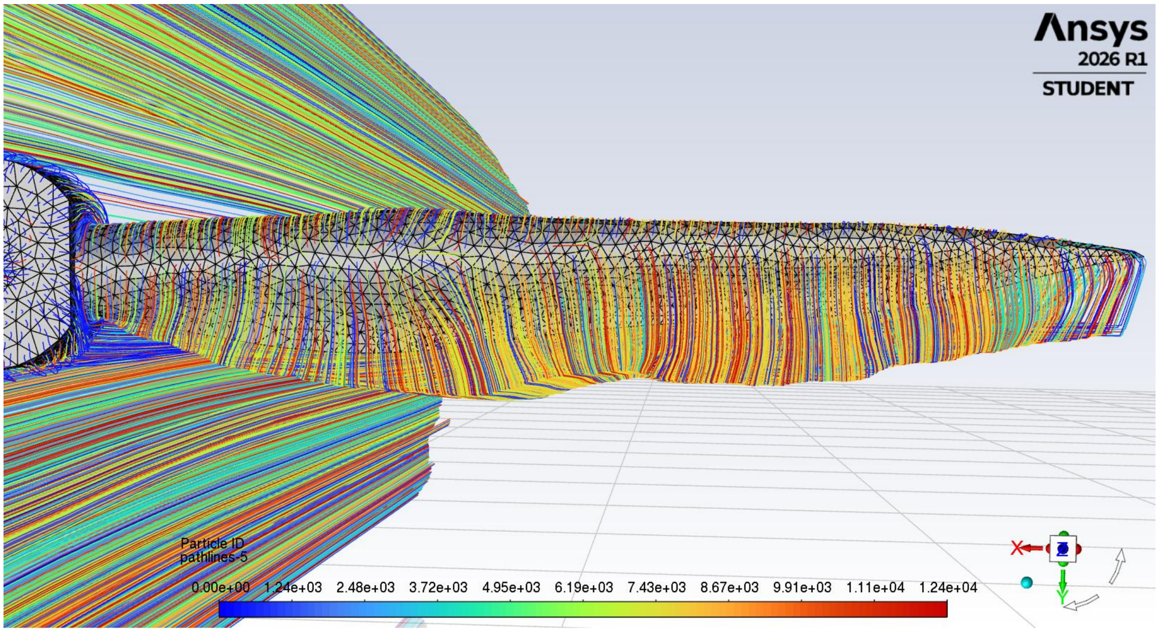

Figure 8: View of Pathlines along Wing

Figure X shows the particle pathlines over the blade surface at 370 rad/s, coloured by particle ID to distinguish individual flow paths. The image clearly shows the airflow dividing at the leading edge of the NACA 4412 profile, paths travelling over the upper (suction) surface and beneath the lower (pressure) surface.

The suction surface is more curved, forcing the air to travel a longer path and accelerate, reducing local static pressure. The pressure surface is flatter, producing slower flow and higher static pressure beneath the blade. This pressure differential across the aerofoil generates a lift force perpendicular to the relative wind direction.

4.5 Results

The torque extracted from the ANSYS Fluent moment report:

Component	Torque (Nm)
Pressure	0.005672
Viscous	0.001019
Total	**0.006692**

Mechanical power predicted by CFD:

$$P_{CFD} = T \times \omega = 0.006692 \times 370 = 2{,}476\,mW$$

This is notably close to the Betz limit calculated in Section 3.5 which is 2,854mWs. The CFD result is 86.8% of the Betz limit, corresponding to a power coefficient of C_p = 0.514, just 8% below the theoretical maximum any turbine can achieve. This close agreement is expected since the simulation was run at the optimal TSR, and validates both the blade design and the CFD setup.

5 Experimental Setup

5.1 Bill of Materials

Item	Description	Qty	Price (£)
DC Motor	Used as the Generator on the turbine	1	1.50
Arduino Uno R3	Microcontroller for logging the data	1	22.00
INA219 Sensor Module	Current and Voltage sensor	1	5.00
Breadboard	Solderless prototyping board	2	3.00
LED	Electrical Load Indicator	2	0.10
Clarke CPF18B Fan	Wind Source	1	LE
PLA filament	Material for the blades	20g	0.50
Jumper Wires	To connect components electrically	6	3.00
		TOTAL	**35.10**

5.2 Experimental Setup

The completed turbine assembly was positioned directly in front of the Clarke CPF18B fan (around 5cm Infront), with the rotor face perpendicular to the airflow. The fan was set to full speed, producing the calculated inlet velocity of 6.26 m/s at the rotor disc.

The DC motor housed in the nacelle was connected via leads running down to the INA219 current and voltage sensor, allowing simultaneous measurement of voltage, current, and power. The Arduino Uno R3 was programmed to sample the INA219 every one second and output readings in

CSV format via the Serial Monitor, logging elapsed time (s), voltage (V), current (mA), and power (mW).

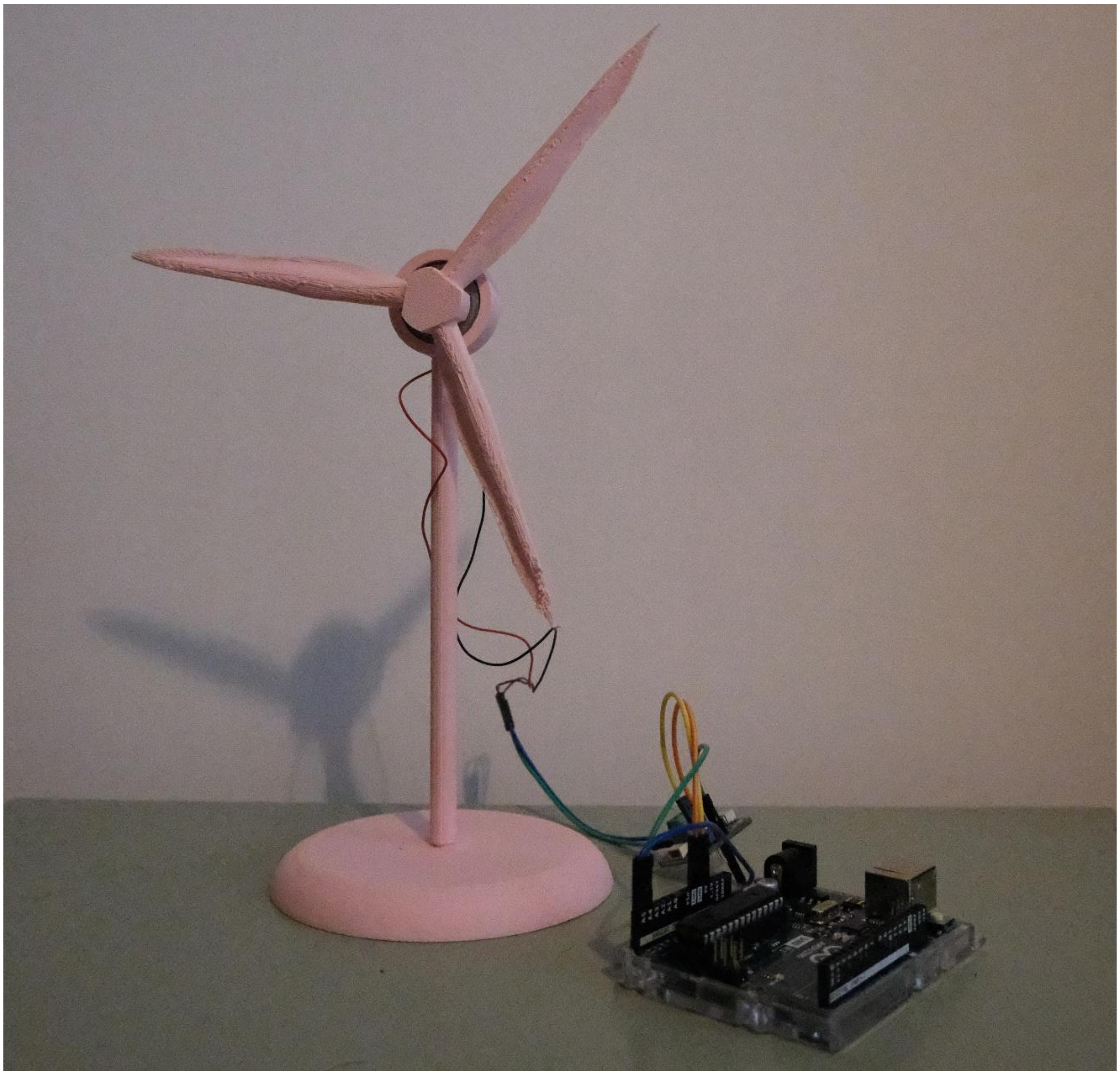

Figure 9: Physical Experiment Setup

Data was collected over a continuous test run and subsequently exported and analysed in MATLAB.

5.3 Results

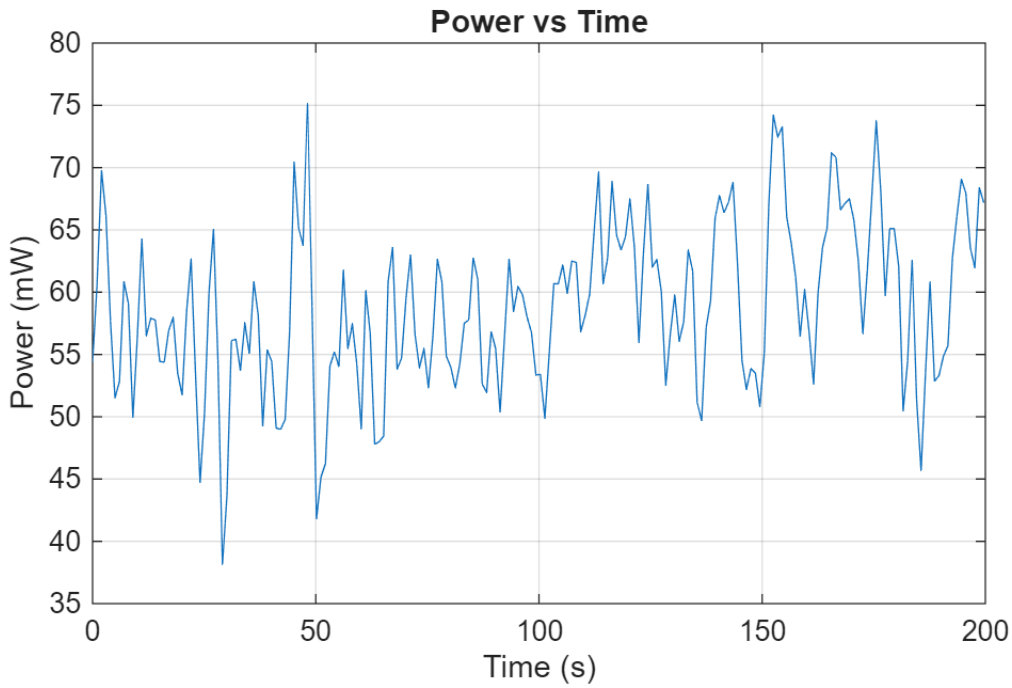

Figure 10: Power Vs Time

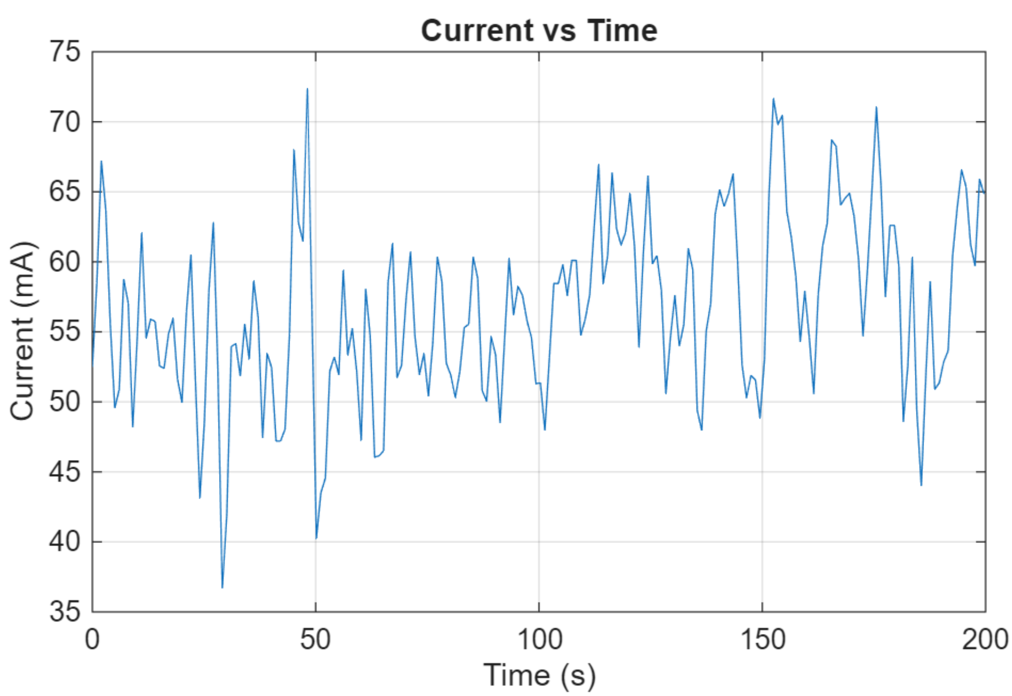

Figure 11: Current Vs Time

Figures 10 and 11 show the electrical power and current output logged by the Arduino over the 200-second test run. Both signals show significant oscillation throughout, ranging from 38–75 mW for power and 37–72 mA for current. This variability is attributed to turbulence in the near-field fan airflow and the electromechanical characteristics of a small brushed DC motor.

Despite the fluctuations, the output remained broadly stable across the full test duration with no significant drift, indicating consistent turbine operation throughout. Overall, our results show a generated; mean power output of 58.73 mW, mean current generated 56.58 mA all over a test duration of 200s.

5.4 Efficiency Analysis

The three-way power comparison between theoretical, CFD, and experimental results is summarised below:

	Power (mW)
Betz Limit (theoretical limit)	2,854.00
CFD Prediction (370 rad/s)	2,476.00
Measured Electrical Output	**58.73**

The measured output of 58.73 mW is significantly lower than the CFD prediction of 2,476 mW. Overall system efficiency relative to the Betz limit:

$$\eta_{overall} = \frac{58.73}{2{,}854} = \mathbf{2.1}\%$$

6 Discussions

6.1 Sources of Efficiency Loss

The measured electrical output of 58.73 mW represents just 2.4% of the CFD-predicted shaft power of 2,476 mW. This large gap is expected for a small-scale prototype and can be attributed to several compounding loss mechanisms:

The CFD simulation was run at 370 rad/s, the theoretical optimal speed for TSR = 6. In practice, the DC motor acting as a generator imposes a resistive torque on the shaft, slowing the turbine significantly below this speed. At lower RPM, the turbine operates at a much reduced TSR, well below the optimal value of 6, meaning the blades are generating far less aerodynamic torque than the CFD predicts.

A brushed DC motor was used as the generator. These motors are poorly suited to low-speed generation, at low RPM, brush friction losses and copper I^2R losses are large relative to the small power output, resulting in poor electromechanical conversion efficiency.

FDM 3D printing produces visible layer lines on the blade surface. At high Reynald Numbers, the boundary layer is laminar and highly sensitive to surface roughness. The rough PLA surface likely triggers early boundary layer transition or separation, increasing drag and reducing lift relative to the smooth aerofoil assumed in CFD.

The turbine was placed directly in front of the fan in its near-field turbulent zone. The CFD assumed a uniform 6.26 m/s inlet — in reality the fan produces a swirling, non-uniform velocity profile that reduces effective power extraction and increases unsteady loading.

6.2 Future Improvements

Several targeted improvements could substantially increase system efficiency in future iterations:

Post-processing the 3D printed blades by sanding and applying a smooth finish would reduce surface roughness and restore laminar flow over the suction surface, directly improving lift-to-drag ratio.

Replacing the DC motor with a purpose-built permanent magnet synchronous generator (PMSG) designed for low-speed operation would significantly improve electromechanical conversion efficiency, as PMSGs have no brush losses and are optimised for the low RPM range relevant to small turbines.

Adding an MPPT circuit between the generator and load would dynamically match the electrical load impedance to the generator's output impedance, ensuring maximum power transfer at all operating speeds.

Extending blade length beyond the current 95 mm printer limit — for example using a larger format printer or assembling multi-section blades — would increase swept area and available wind power cubically with radius.

Replacing the industrial fan with a wind tunnel would provide a controlled, uniform inlet flow matching the CFD boundary conditions more closely, isolating aerodynamic performance from flow quality effects.

7 Conclusion

This project successfully completed a full engineering cycle for a small-scale horizontal axis wind turbine, from aerodynamic theory and CAD design, through CFD simulation and physical fabrication, to instrumented experimental testing and data analysis.

A three-bladed HAWT was designed in Fusion 360 using the NACA 4412 aerofoil profile, with a blade span of 95 mm and total tip radius of 101 mm. The design was 3D printed in PLA and tested in a controlled airflow of 6.26 m/s produced by a Clarke CPF18B fan. Electrical output was measured using an INA219 sensor and Arduino Uno R3, logging data at one-second intervals over a 200-second test run.

The theoretical Betz limit for this turbine was calculated as 2,854 mW. CFD analysis in ANSYS Fluent at the optimal operating speed of 370 rad/s (TSR = 6) predicted a shaft power of 2,476 mW, corresponding to a power coefficient of 0.514, 86.8% of the Betz limit, validating both the blade design and the simulation setup. The measured electrical output of 58.73 mW reflects real-world losses from generator inefficiency, operating speed mismatch, blade surface roughness, and non-uniform inlet flow, giving an overall system efficiency of 2.1% relative to the Betz limit.

These results are consistent with published data for small-scale educational prototypes and demonstrate that the primary performance bottleneck lies in electromechanical conversion rather than aerodynamic design

The project demonstrated practical application of fluid mechanics, CAD modelling, CFD analysis, and embedded systems within a single integrated prototype. achieving all stated objectives.

References

[1] Abbott, I. H. & von Doenhoff, A. E. (1959). *Theory of Wing Sections.* Dover Publications.

[2] Ada, L. (2012, October 26). *Adafruit INA219 Current Sensor breakout*. Adafruit Learning System.

[3] IRENA (2023). *Renewable Power Generation Costs.*

[4] Autodesk Inc. (2024). *Fusion 360.*

[5] Hansen, M. O. L. (2015). *Aerodynamics of Wind Turbines*, 3rd ed. Routledge, London.

[6] Manwell, J. F., McGowan, J. G. & Rogers, A. L. (2009). *Wind Energy Explained: Theory, Design and Application*, 2nd ed. Wiley, Chichester.

[7] Clarke International (2023). *CPF18B 18" Professional Floor Fan — Product Specification Sheet*. Clarke International Ltd., Essex.